Journal of Fluids and Structures (1999) **13,** 907–933
Article No.: jfls. 1999.0247, available online at http://www.idealibrary.com on IDEAL®

PRESSURE AND FORCE FLUCTUATIONS ON ISOLATED ROUGHENED CIRCULAR CYLINDERS OF FINITE HEIGHT IN BOUNDARY LAYER FLOWS

A. KAREEM

NatHaz Modeling Laboratory, Department of Civil Engineering & Geological Sciences, University of Notre Dame, Notre Dame IN 46556-0767, U.S.A.

AND

C. M. CHENG

Department of Civil Engineering, Tamkang University, Taipei, Republic of China

(Received 13 November 1998 and in revised form 28 July 1999)

This paper presents spatio-temporal measurements of a fluctuating pressure field acting on isolated roughened cylinders of finite height in simulated turbulent boundary layer flows at subcritical Reynolds numbers. The cylinder surface is roughened by placing discrete roughness elements along the height at four circumferential locations. The resulting surface roughness configuration helps to modify the flow over the cylinder, which leads to the pressure field that exhibits characteristics similar to the transcritical Reynolds numbers. The space-time measurements of the random pressure field allowed computations of the mean and r.m.s. pressure coefficients, power spectral density, spanwise and circumferential correlations, and their eigenfunction expansions. A manifold-pneumatic averaging technique was utilized to evaluate time varying area-averaged loads at various levels along the model height. The spatially averaged measurements of the pressure field over the roughened cylinder facilitated the estimation of local and mode-generalized alongwind and acrosswind aerodynamic force coefficients, their spectral descriptions and multi-level force correlations. An increase in the turbulence level influences the fluctuating pressure field through modifications which take place in the structure of the boundary layer over the cylinder and the structure of the separated shear layers.

1. INTRODUCTION

STUDIES CONCERNING HIGH REYNOLDS number flows around circular cylinders are limited due to difficulty in simulating these flow features in wind tunnels [e.g. Trunstall (1970), Achenbach & Heinecke (1981), Schewe (1983), Shih *et al.* (1993), Van Nunen (1972)]. The difficulty in achieving transcritical Reynolds number flows around bodies with circular cross-sections has led to a large body of data in which roughened cylinders have been utilized to artificially simulate these flow effects. From flow pattern studies, it is known that the major difference between the subcritical and transcritical regions is that the former has a laminar separation at an earlier stage, i.e. at a smaller angle. Therefore, changing the subcritical flow pattern to a transcritical one would either cause the transition of laminar boundary layer to turbulent layer, or simply prevent early separation. The transition of the laminar boundary layer prior to its separation helps the fluid gain more momentum, which leads to separation at a later stage. This can be accomplished by introducing high-intensity,

0889–9746/99/100907 + 27 $30.00

small-scale turbulence into the free stream. The other alternative involves disturbing the laminar boundary layer by adding artificial roughness on the model surface (Figure 1). Both approaches have merits and shortcomings.

The effects of free-stream turbulence on the characteristics of flow around a circular cylinder are complex and can be classified in terms of intensity and length scale of turbulence. For many decades, the effect of free-stream turbulence on the flow patterns in the vicinity of a circular cylinder (e.g. cause transition of Reynolds number, delay the flow separation, and reduce the mean drag coefficient) has been recognized. The small-scale turbulence in the same order of magnitude as that of the cylinder boundary-layer thickness plays an important role. A laminar boundary layer could become turbulent and gain enough momentum to overcome more adverse pressure gradients and delay the separation which causes the Reynolds number transition (Bruun & Davies 1975; Batham 1973; Surry 1972). In contrast with the small-scale effects, the large-scale turbulence does not energize the cylinder boundary layer, and can be viewed as a slow variation of the mean velocity in the free stream. It is also important to note that for the small-scale turbulence to have a significant influence on the Reynolds number transition, the flow Reynolds number must be in the range of 10^5 (Sadeh & Saharon 1982).

The effects of surface roughness on Reynolds number were recognized as early as 1930. Fage & Warsap [quoted by Schlichting (1960)] and Szechenyi (1975) showed a steady decrease in the critical Reynolds number as the roughness increased. Since 1970, Achenbach & Heinecke (1981), Batham (1973), Farell (1981) and Guven *et al.* (1980) have studied the effect of uniformly distributed surface roughness on the pressure distribution, drag and lift coefficients, and vortex shedding on circular cylinders. Nakamura & Tomorai (1982) and Guven *et al.* (1980) noted that, for a given roughness arrangement, a value of the Reynolds

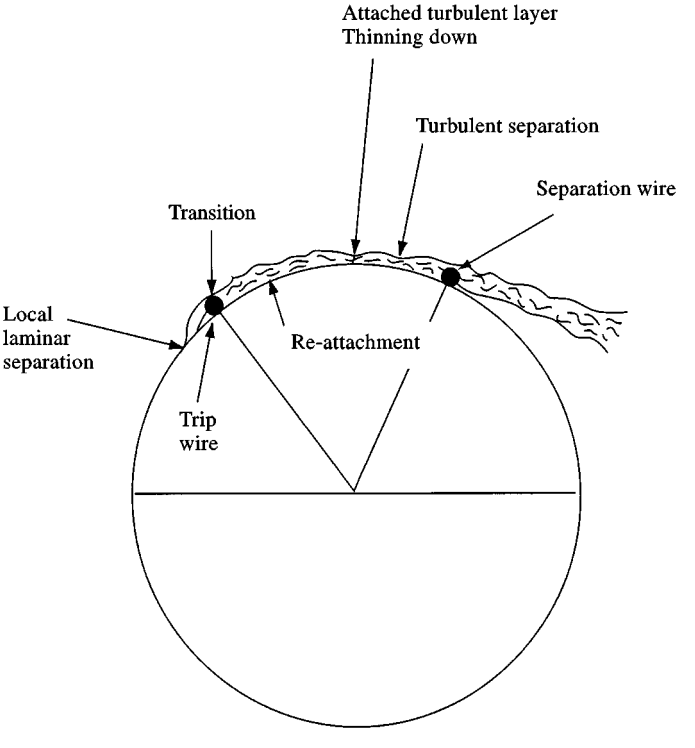

Figure 1. A schematic of flow around circular cylinders with roughness wires.

number could be found at which the aerodynamic characteristics become independent of the Reynolds number. Using the ESDU database, Lawson (1982) noted that with the proper form of roughness elements, a transcritical Reynolds number flow field can be simulated at Reynolds numbers as low as $2{\cdot}72 \times 10^4$. Some later studies demonstrated that by using multiple two-dimensional ribs as the roughness elements, Reynolds number independence can be achieved at lower Reynolds numbers (Guven *et al.* 1980). Nakamura & Tomorai (1982) discovered that applying a "strip" of roughness at $\theta = 50^\circ$ rather than uniformly covering the entire model could produce Reynolds number independence. Schnabel (1981) used a pair of roughness wires to disturb the laminar boundary layer, which caused the transition to the turbulent boundary layer. Naumann & Quadflieg (1972) went one step further by adding an additional pair of wires for roughness where the boundary layer separates from the cylinder surface at transcritical Reynolds numbers (Figure 1). Recently, Shih *et al.* (1993) reported the results of an experimental study of flow past rough circular cylinders at large Reynolds numbers utilizing a pressurized wind tunnel at NASA Ames. This study was conducted using a two-dimensional model. However, the flow features were not reported in the reference. It appears that the results pertain to smooth approach flow conditions.

Most of these studies were conducted either for two-dimensional cylinders or for finite height cylinders where only limited characteristics of the pressure field were monitored. The present study concerns a detailed set of measurements of the space-time structure of pressure fluctuations on finite height cylinders. Two-dimensional discrete surface roughness elements were placed at optimal circumferential positions on the cylinders. A manifold-pneumatic averaging technique was utilized to evaluate time-varying area-averaged loads at various heights along the model. The spatially averaged measurements of the pressure field facilitated the estimation of local and mode-generalized aerodynamic loads, their spectral description, and multi-level force correlation.

2. EXPERIMENTAL

All measurements were made in a boundary-layer wind tunnel at the University of Houston in two simulated approach flows referred to as a BLI and BLII. The wind tunnel has a test-section 60 ft (18·29 m) long with a cross-section of 10 ft × 5 ft (3·05 m × 1·52 m) at the model location. The similarity requirements for simulating a turbulent boundary layer in a wind tunnel were obtained from dimensional arguments derived from the conservation laws applicable to the lower atmosphere (Cermak 1971). Different combinations of floor roughness devices, barriers and spires at the entrance to the test-section were utilized (Kareem *et al.* 1989). The kinematics of the turbulent-flow fields associated with BLI and BLII flows are similar to those of an open terrain and urban conditions, respectively. Details concerning the kinematics of these boundary layers are given in the next section.

A rigid Plexiglas model 3 in (76·2 mm) in diameter and 30 in (76·2 mm) in height with five levels of measurement was built. Each level was fitted with 12 taps. Rotating the turn table 10° in either direction permitted measurements at 10° intervals. In Table 1, details concerning the vertical tap locations are provided. These taps were connected to the electronic pressure transducers via 1/16 in (1·59 mm) diameter flexible tygon tubing. The length of each tube was kept at 36 in (914 mm) to minimize the calibration and data reduction efforts.

The second type of model used in this study was designed to study area-averaged pressures reflecting two orthogonal force components, i.e. alongwind and acrosswind. Geometrically, the model is identical to the pressure model described earlier. The pressure taps at each level were circumferentially located in a manner so that differencing the manifold pressure on each half of the cross-section would yield a resultant force. A total of

TABLE 1

Distribution of pressure tabs

Levels	Pressure model z (in)	Force model z (in)
1	29·0	28·42
2	23·0	25·04
3	17·0	21·11
4	11·0	16·20
5	5·0	6·71

five levels were installed for pneumatic averaging (Table 1). In this manner, the summation of pneumatically averaged area loads at five levels provided the mode-generalized load for subsequent dynamic analyses (Kareem *et al.* 1989).

In the pneumatic averaging technique, the pressure field is sensed through discrete pressure taps located on the model surface. The taps are as closely spaced as permitted by the size of the model and required by the inhomogeneity of the surface pressure field. This averaging procedure correctly accounts for the lack of spatial coherence of the pressure field fluctuations over an area through differences in correlation or phase. If the spacing between pressure taps exceeds certain wavelengths of pressure fluctuations, the resulting force will be overestimated in the frequency range corresponding to these wavelengths.

In this study, each level of measurement was divided into two semicircles. Each semicircle had seven pressure taps which were weighted such that the tributary arc length for each tap resulted in an identical value of $\sin\theta \mathrm{d}\theta$, in which θ is the angle between the axis dividing the two semicircles and the line joining the tap location on the circumference and the origin, and $\mathrm{d}\theta$ is the arc angle subtended by the tributary arc length. The chordwise angular locations θ of the taps on a semicircle are 34, 56, 74, 90, 106, 124 and 146°. Each of the seven-tap group was connected to a seven-input manifold. The two manifolds facing opposite sides were differenced by an electronic pressure transducer to obtain lateral loads at that level. Similarly, the mode-generalized aerodynamic loads on the cylinder were derived by nonuniform spacing of the five levels of measurement along the cylinder elevation. These levels were determined such that for each level, the product of the tributary area and the linear mode shape at that level resulted in a constant value. In this manner, a summation of the resultant manifold pressure at each level after multiplication with an appropriate area constant would provide the mode-generalized loading. Further details can be found in Kareem & Cheng (1984).

Any pressure measurement involving the tubing system introduces additional dynamics in the overall measurement system. The dynamic features of a tubing system are needed for reliable interpretation of the measured signal. The pneumatic system should be designed to transmit the surface pressure field with minimum amplitude modification, i.e. attentuation or amplification, to the pressure transducer. A phase lag is inherent in such measurements; the design objective is that it should remain linear within this frequency range of interest. In this manner, the frequency-amplitude characteristics of pressure fluctuations are preserved, with the exception of a fixed time delay. It is desirable to use symmetric manifolds and tubing of identical lengths and geometry to avoid the introduction of undesirable weighting of the pressure field. The calibration of both individual tubing and manifolds is essential for ascertaining the dynamic characteristics of the pneumatic system. Details concerning these calibrations have been reported by the authors in Kareem *et al.* (1989).

Two types of discrete roughness elements were utilized for this study. Some roughness elements were selected based on their ability to reproduce the mean pressure distribution close to high Reynolds number flows. Other roughness elements tested included various sizes of wires at different angles, uniformly distributed wires, wires with different sizes and spacings intervals, irregular arrangement of wires, and combinations of sand papers and wires. The optimal roughness details found for the conditions in this study are the following:

3-I: 3 in × 30 in smooth cylinder;
3-II: 3 in × 30 in model 0·02 in wire at $\pm 65^\circ$ and 0·06 in at $\pm 115^\circ$, each wire continuous 30 in in length;
3-III: 3 in × 30 in model 0·02 in wire ± 60, $\pm 65^\circ$ and 0·06 in at ± 110, $\pm 115^\circ$, each wire 3 in in length. This roughness configuration is stagged to break-up possible two dimensionality of the flow caused by long two-dimensional elements.

In 3-III the lengths of the wires were limited to 3 in, and were staggered. The wires were placed near the top, similar to 3-II, but with a length of 3 in. A $\pm 5^\circ$ shift was then added to alternating 3-in segments.

The output of the pressure transducers (Setra-237) was fed through a signal conditioning unit before being digitized and recorded on magnetic storage media. The sample length was 300 s and was recorded at a rate of 250 samples/s. The data were then reduced to obtain spectral and statistical characteristics of the point- and area-averaged pressure fluctuations.

The overall accuracy of measurements is expressed in terms of repeatability. Although not a measure of absolute accuracy, it provides an assessment criterion for accuracy. The overall repeatability in terms of a local pressure coefficient was 0·1 for the mean pressure and 0·03 for the r.m.s. coefficient. The drag coefficient, which is an integral of the mean pressure distribution, showed repeatability with 0·3%. The normalized standard error in the spectral estimates was found to be 0·075–0·105. The mean free-stream velocity was repeatable within $\pm 3\%$ of the free mean velocity. The measurements of mean velocity and local turbulent intensity were repeatable to within ± 3 and $\pm 6\%$ of the value measured, respectively. Additional details can be found in Kareem *et al.* (1989).

3. RESULTS AND DISCUSSION

The single- and multi-point analysis of the pressure field provided information on the mean and r.m.s. pressure distributions, power spectral density functions, spanwise and chordwise narrow- and broad-band correlations, and orthogonal expansion of the pressure field into eigenvectors. The spatially averaged measurements of the pressure field facilitated the estimation of local and mode-generalized aerodynamic force coefficients, their spectral descriptions, and multi-level force correlation. The Reynolds numbers at which this study was conducted varied between $2{\cdot}54 \times 10^4$ and $2{\cdot}75 \times 10^4$.

3.1. Flow Field Characteristics

The mean wind velocity and local turbulence intensity profiles as functions of nondimensional height are presented in Figure 2 for BLI and BLII flows. In BLI, there is less variation of the incident mean velocity along the model elevation and a lower intensity of turbulence than in BLII. The shape factors of the boundary layers (δ_d^*/θ_d, where δ_d^* and θ_d are the boundary layer displacement and momentum thickness, respectively) were estimated to be 1·46 and 1·69 for BLI and BLII, respectively. The longitudinal length scale between heights of 10 and 30 in varied from 12 to 20 in. Accordingly, the ratio of the turbulence length scale to the model diameter varied between approximately 4 and 7.

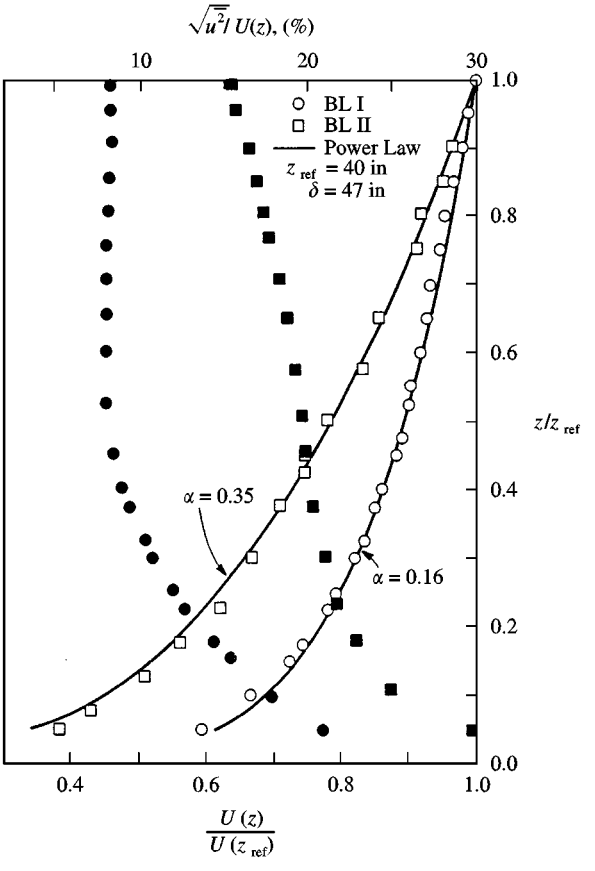

Figure 2. Mean velocity and turbulence intensity profiles for BLI and BLII flows.

3.2. Mean and Fluctuating Pressure Distribution

The results for the circumferential mean pressure coefficient distributions are given in Figure 3. These distributions show good agreement with high Reynolds number flow cases, e.g. $\bar{C}_{p_{\min}} = -1{\cdot}75 \sim 1{\cdot}85$, $\bar{C}_{p_b} = -0{\cdot}52$ to $-0{\cdot}56$, $C_D = 0{\cdot}55 \sim 0{\cdot}63$. The Strouhal number for simulated high Reynolds number flows is between 0·18 and 0·2, depending on the flow condition. The results are also compared with high Reynolds flow data obtained in both laboratory and full-scale environments, which show agreement with these studies (Figure 3). The pressure distribution also provides good comparison with the recent wind tunnel study reported by Shih *et al.* (1993). The separation angle is defined as the location where the pressure coefficient has recovered halfway to the base pressure coefficient. The separation angle is found to be approximately 110–120°, which is in agreement with related studies referenced in the paper. The measured values of the mean pressure coefficients, drag coefficient, and the separation angle clearly indicate that the discrete surface roughness configuration utilized in this study can simulate high Reynolds number flow features at low Reynolds number flows. Table 2 summarizes the results, including those obtained using the smooth cylinder (3-I).

The r.m.s. pressure distribution around the cylinder is given in Figure 4. The r.m.s. pressure coefficients at the stagnation point are in good agreement with the strip and quasi-steady theories. The unusual presence of peaks in the distribution at around $\theta = 70°$

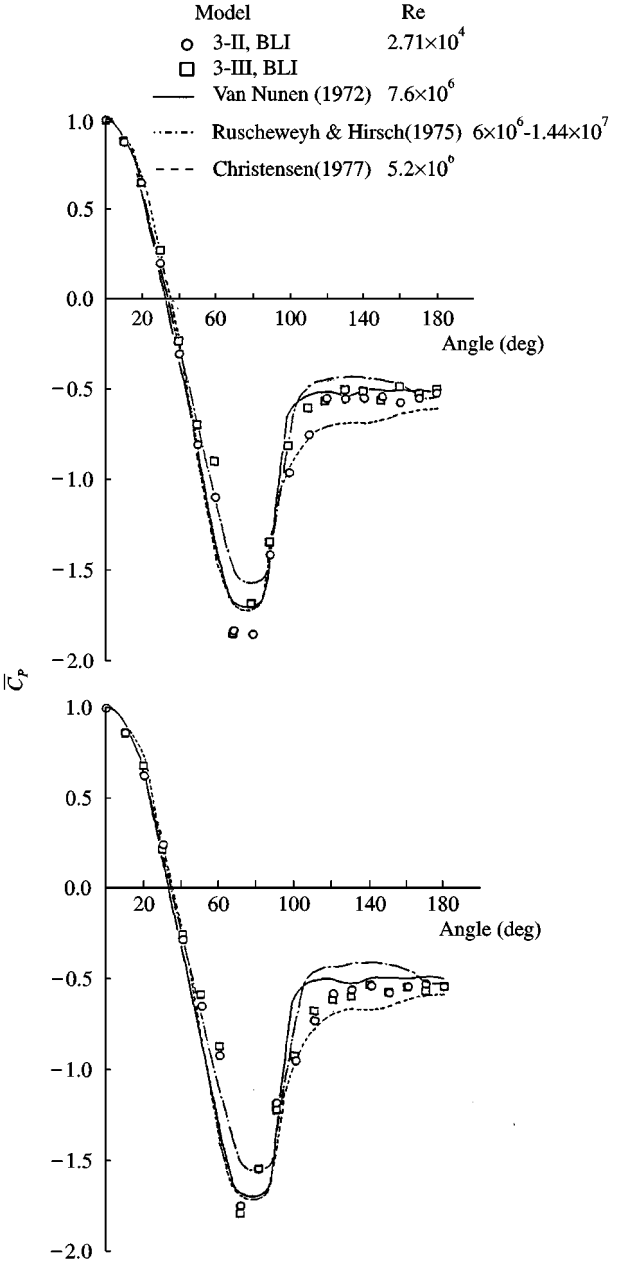

Figure 3. Mean pressure distribution at level 3 (defined in Table 1).

is noted. The peak is slightly less dominant for flow around cylinder 3-III than around 3-II due to the staggered configuration. This peak appears to be due to the local effect of the first surface roughness wire which is located just upstream of the pressure tap at 70°. The pressure measurements conducted over forward and backward step configurations show such sharp peaks [e.g. Farabee & Casarella (1986)].

TABLE 2

Aerodynamic characteristics

Model	Boundary layer	Re (10^4)	C_D	$\bar{C}_{P_{min}}$	$\bar{C}_{P_b}$	S
3-I	I	2·71	0·81	−0·74	−0·58	0·147
3-II	I	2·66	0·55	−1·85	−0·55	0·215
3-III	I	2·71	0·56	−1·84	−0·52	0·200
3-I	II	2·53	0·90	−0·88	−0·72	0·151
3-II	II	2·56	0·61	−1·75	−0·56	−0·180
3-III	II	2·54	0·63	−1·80	−0·56	0·182

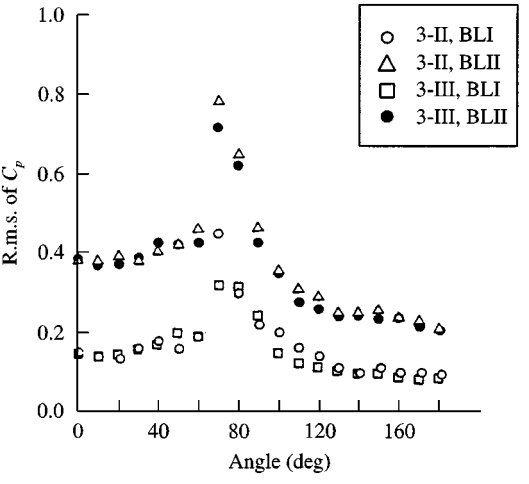

Figure 4. R.m.s. pressure distribution at level 3 (defined in Table 2).

3.3. POWER SPECTRAL DENSITY

In Figures 5 and 6, the reduced power spectral density functions of the circumferential pressure fluctuations for roughness configurations 3-II and 3-III for both flow conditions are presented. These plots indicate vortex shedding peaks at frequencies corresponding to the Strouhal number of 0·215 and 0·18 in BLI and BLII, respectively. These values are in good agreement with the full-scale measurements on chimneys (Christensen 1977; Muller & Nieser 1976) and are in contrast with those observed for the smooth flow (Table 2). It is also noted that the spectra show a sudden increase of low-frequency components at $\theta = 70$ and 80°. This trend is more pronounced for the 3-II case in comparison with 3-III. The measurements around both the forward and backward steps show the presence of low-frequency energy (Farabee & Cassarella 1986). The presence of a roughness wire on the smooth cylinder surface is similar to a flow over a step. As the fluid convects downstream of the wire, the low-frequency contents of the pressure spectra decrease. A careful observation of Figure 5 also suggests that the vortex shedding peak disappeared or was seriously weakened at $\theta = 80°$ for roughness configuration 3-II. A similar observation was made by Batham (1973) in supercritical Reynolds numbers and was associated with the appearance of separation bubbles. However, in 3-III, this was not observed. In both the 3-II and 3-III roughness cases, introduction of turbulence eliminated peaks for pressure taps from 0 to

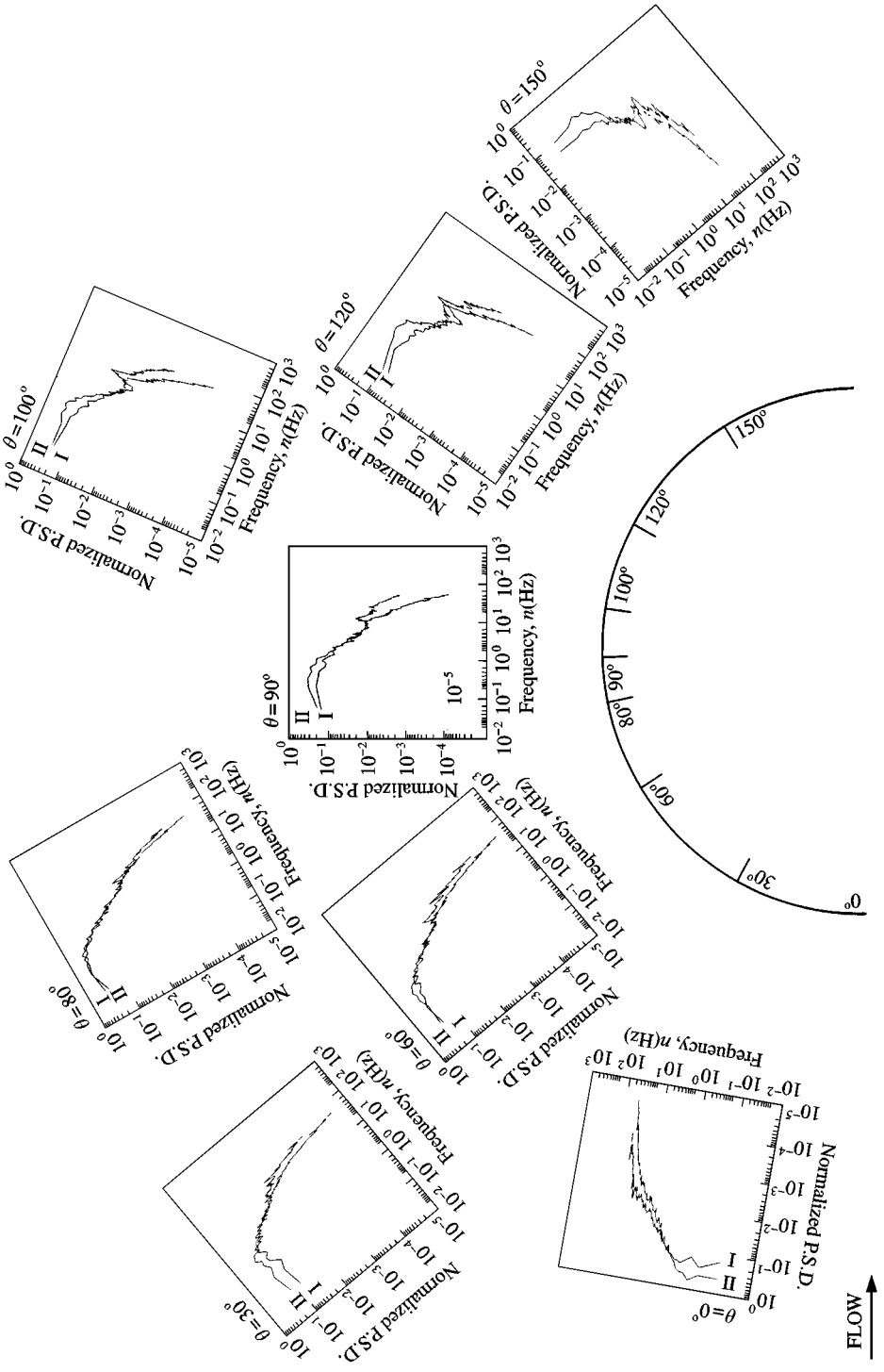

Figure 5. Power spectral distribution of pressure fluctuation at level 3 (see Table 1) of 3-II in BLI and BLII.

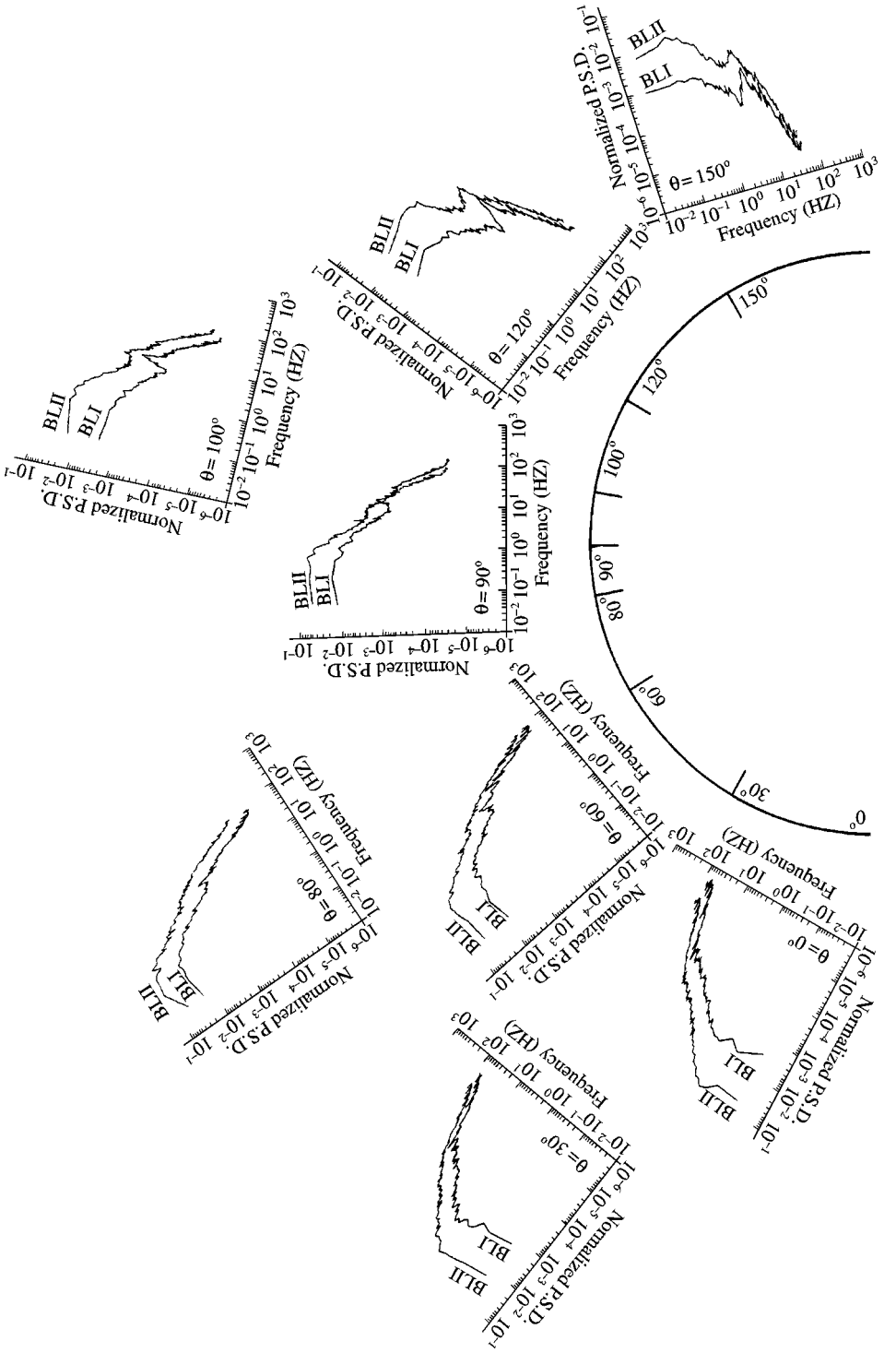

Figure 6. Power spectral distribution of pressure fluctuation at level 3 (see Table 1) of 3-III in BLI and BLII.

80°. For taps at angles of 90–180°, the peaks related to vortex shedding were broadened, and a reduction in the amplitude of peaks and a slight reduction in the Strouhal number was noted. With the exception of localized effects in the wake of the separation wire, the results suggest that after flow separation from the first pair of wires, it reattached to the surface immediately and did not form a long separation bubble as in the supercritical flows. Subsequently, the energized reattached fluid then separated at a separation angle of approximately 115°, which corresponds to the supercritical flows.

3.4. Circumferential Pressure Correlation

The circumferential pressure correlation coefficients, $R_{\theta\phi}$, in which θ is the reference point and ϕ is the angle of circumferential separation, were measured at a spacing interval of 30°. In Figures 7 and 8, circumferential pressure correlations for models 3-II and 3-III in BLI and BLII are given. The circumferential correlation distribution is qualitatively quite similar in both cases, with some differences in magnitude. A negative lobe in the distribution of $R_{\theta\phi}$, for $\theta = 0°$ is noted for all model surface configurations and flow conditions. The trend is more distinct in BLII flow than in BLI flow, implying that the pre-separation region exhibits negative correlation with the separated region. The results also suggest higher circumferential correlation in the separated region for both flow conditions. The correlation function reflects the circumferential distribution of the mean pressure. This trend has also been observed in a two-dimensional cylinder study (Batham 1973). The strong antisymmetric distributions of pressure reported in the literature involving two-dimensional cylinders exposed to low turbulence intensity and/or small-scale turbulence are less prominent in this study. The effect of increased turbulence is to vitiate the antisymmetric pressure distribution induced by vortex shedding.

3.5. Spanwise Pressure Correlation

The spanwise pressure correlations were measured at spanwise generators located at $\theta = 60$, 90 and 120° by simultaneously monitoring pressure along a generator. The correlation measurements included broad-band correlation that encompassed the entire frequency range influenced by the free-stream turbulence and vortex shedding. Narrow-band correlations were obtained in order to isolate the influence of vortex shedding. This was done by evaluating the co-spectral density function peak at the vortex shedding frequency. Howell & Novak (1979) and Kareem (1978) noted that, unlike tests conducted using two-dimensional cylinders in uniform flow, the correlation coefficients were dependent on the reference point for the three-dimensional cylinder in turbulent boundary layer flow. This implies that they are non-homogeneous. The reference pressure tap was kept fixed at $2.33D$ from the top for each case where the free-end effects are diminished. The broad- and narrow-band correlations are presented in Figures 9 and 10. The results include the smooth cylinder cases (3-I).

The broad-band correlation length scales for both the 3-II and 3-III cylinders is largest at $\theta = 120°$, as compared with $\theta = 60$ and 90° in BLI (Table 3). A change in the approach flow to BLII increases the correlation length up to one cylinder diameter in the pre-separation regions, i.e. $\theta = 60$ and 90° with a smaller increase at $\theta = 120°$. This suggests that the pressure correlation length in the pre-separation part of the cylinder tended to reflect more the length scale of the free-stream turbulence than the wake region. The fact that the correlation for the 3-II and 3-III configurations does not differ significantly indicates that either the stepping roughness element (3-III) was unable to break the two-dimensional wake flow pattern, or the wake was already three-dimensional in the 3-II case. Sageau (1978)

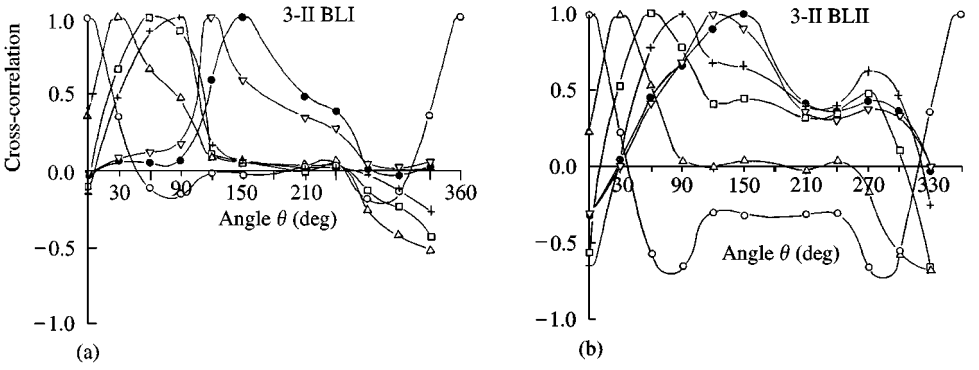

Figure 7. Circumferential pressure correlation of pressure at level 3 (see Table 1) for 3-II cylinder (a) BLI and (b) BLII.

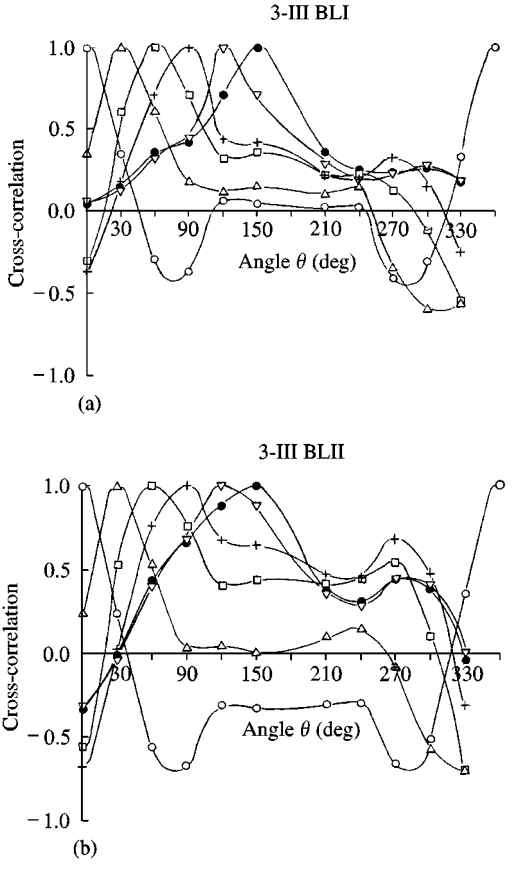

Figure 8. Circumferential pressure correlation of level 3 (see Table 1) for 3-III cylinder: (a) BLI and (b) BLII.

reported a correlation length of $2D$ at $\theta = 100 \sim 110^\circ$ from a full-scale chimney located in an open terrain. This is in agreement with the cylinder 3-II in BLI. This observation reinforces the earlier statement that the pressure field simulated by placing discrete two-dimensional wires on the cylinder surface portrays the three-dimensional characteristics of the wake found in full-scale studies at high Reynolds number flows.

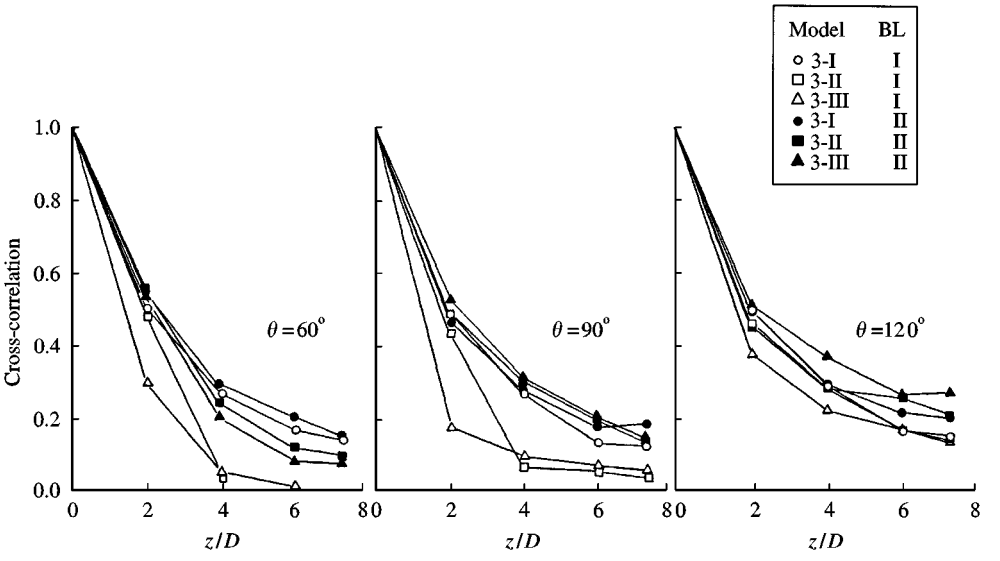

Figure 9. Broad-band spanwise correlations for BLI and BLII.

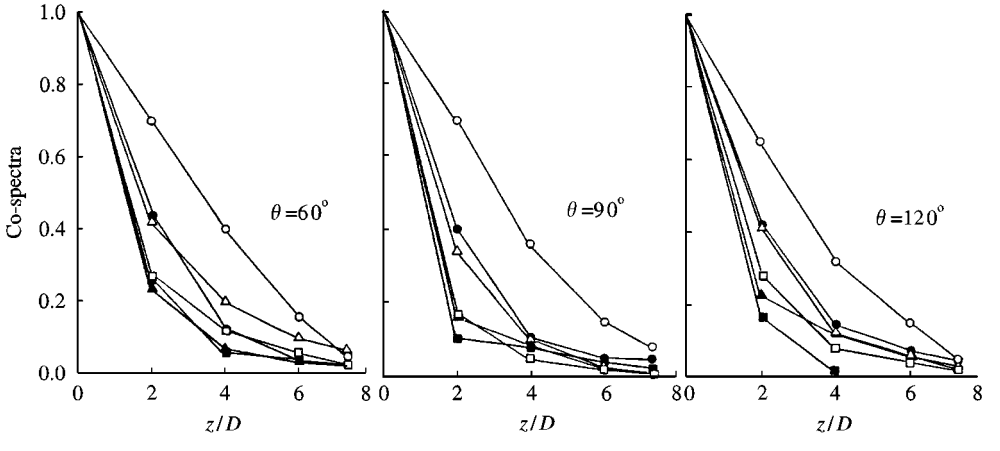

Figure 10. Narrow-band spanwise co-spectra for BLI and BLII (for legends see Figure 9).

The results reported in Table 3 show that the narrow-band correlation length decreases with an increase in free-stream turbulence in both subcritical flow and simulated transcritical flow. It confirms Surry's report that the free-stream turbulence (large scale in this case) would tend to diminish the spanwise coherence of vortices. The measured correlation lengths, $L_p \approx 3{\cdot}4D$ for BLI and $L_p \approx 2{\cdot}2D$ in BLII, are greater than the unit diameter reported by Vickery & Clark (1972) but smaller than the $4{\cdot}0D$ reported by Surry (1972). These differences can be attributed to the experimental conditions that were different in the studies, e.g. the length scale of the free-stream turbulence, turbulence intensity, the presence of a mean velocity gradient, and the effects of flow over the top of the cylinder (Kareem *et al.* 1989). Also, the results indicate that the free-stream conditions had less effect on the narrow-band correlation length in the simulated high Reynolds number flow than in the

TABLE 3

Spanwise pressure length scale

Model	Boundary layer	Broad-band L_p/D			Narrow-band L_p/D		
		60°	90°	120°	60°	90°	120°
3-I	I	2·92	2·84	2·92	3·50	3·42	3·22
3-II	I	1·99	2·13	2·83	1·89	1·46	1·79
3-III	I	1·71	1·72	2·53	2·45	1·79	2·17
3-I	II	3·15	2·91	3·06	2·22	2·12	2·31
3-II	II	2·89	3·02	3·02	1·72	1·42	1·38
3-III	II	2·68	3·14	3·35	1·68	1·54	1·84

subcritical flow. The smooth cylinder case 3-I exhibits the highest narrow-band correlation lengths in both BLI and BLII.

3.6. EIGENFUNCTION ANALYSIS

The analysis of narrow-banded and wide-banded correlation functions discussed in the preceding section helps to delineate the influence of vortex shedding and incident turbulence on the fluctuating pressure field over the cylinder. Additional insight into the nature of fluctuations can be obtained by decomposing the covariance of the random pressure field along the circumferential and spanwise directions into orthonormal eigenfunctions using an extremum principle (Lumley 1965; Armitt 1968; Kareem & Cermak 1984). Following Mercier's theorem and the Karhunen–Loève expansion, a pressure time history may be expanded in optimal orthogonal functions (Davenport & Root 1958; Loève 1977) as

$$P(x, t) = \sum_{n=1}^{N} a_n(t)\Phi_n(x),$$

in which

$$\overline{a_n(t)a_m(t)} = \delta_{nm},$$

$$\int_0^L \phi_n(x)\phi_m(x)\,\mathrm{d}x = \lambda_n\delta_{nm}, \quad 0 \le x \le L.$$

In the preceding equation, δ_{nm} denotes the Kronecker delta, and $\phi_n(x)$ and λ_n represent the eigenfunctions and the associated eigenvalues, respectively. This expansion is also known as proper orthogonal decomposition (POD). The orthogonal eigenfunctions are obtained by decomposing the pressure covariance

$$\int_0^L R(x_1, x_2)\phi_n(x_2)\,\mathrm{d}x_2 = \lambda_n\phi_n(x_1).$$

For discrete measurements of the random pressure field, $p(x, t)$, between the interval 0 and L at K locations, with a separation distance of Δx, the preceding integral equation reduces to

$$\Delta x \sum_{h=1}^{K} R(x_g, x_h)\,\phi_n(x_h) = \lambda_n\phi_n(x_g), \quad g = 1, \ldots, K.$$

It can be shown that the integral of the mean-square pressure fluctuations over the surface is equal to the sum of the eigenvalues. Each eigenvalue represents the energy contained in its associated spatial eigenfunction (Armit 1968; Davenport & Root 1958). Each eigenfunction may be assigned physical significance on the basis of its spatial variation. For example, a symmetrical eigenfunction may result from the large-scale incident turbulence, whereas an antisymmetric eigenfunction may be contributed by vortex shedding, the lateral component of turbulence, or fluctuating separation points. The orthogonality condition is satisfied by the symmetric and antisymmetric spatial distribution of the functions. The covariance matrix of the circumferential pressure fluctuations was analyzed to obtain the eigenvalues and eigenfunctions. The calculated eigenvalues and vectors are presented in Table 4 and Figures 11 and 12. In all cases, the first five modes contribute 85–95% of the total energy. Approximately, 51–60% of the overall pressure fluctuations on the cylinder are due to the fundamental symmetric mode in both boundary layers. This function resembles the circumferential distribution of the mean pressure coefficients. Based on the quasi-steady and strip theories, it is obvious that the symmetric shape of this mode results from the large-scale incident turbulence.

The antisymmetric spatial distribution of the second mode represents vortex shedding. The contribution to the total energy in this mode is only 33–35%, and is higher in BLI than in BLII. This corroborates the earlier finding that the addition of incident turbulence tends to vitiate the vortex shedding process. This also suggests that vortex shedding is not as dominant as some earlier studies have concluded. The fourth eigenvector is also antisymmetric and its spatial distribution represents the derivative of the first mode or the mean pressure distribution around the circular cylinder. This conforms to the quasi-steady theory assumptions and represents the contribution of the lateral component of turbulence. The eigenvector analysis of full-scale measurements on a cooling tower, conducted by Armitt (1968), qualitatively supports the results reported here.

3.7. Aerodynamic Force Measurements

Local and generalized fluctuating alongwind and acrosswind aerodynamic loads were measured in both BLI and BLII for only the 3-II case. In Figures 13 and 14, local alongwind and acrosswind load spectra are given. The alongwind spectra are broad-banded and reflect the spectra of the incidence turbulence. Unlike the spectral description of the alongwind loading, the acrosswind load spectra has a relatively narrower bandwidth and contains spectral peaks associated with the Strouhal frequency. The addition of turbulence tends to broaden and reduce the amplitude of the vortex shedding peaks. A slight reduction in the Strouhal number is also noted. This trend reflects the features observed for the single point pressure fluctuations. Similar observations were made in the case of the smooth cylinder (Kareem *et al.* 1989). An examination of the acrosswind force spectra indicated that the vortex shedding peak is modified near the tip region and the level near the tunnel floor. Near the top, this observation can be attributed to downwash from the tip flow which disrupts the organized structure of wake fluctuations. Similar trends were noted by Ayoub and Karamcheti (1982) and Kareem *et al.* (1989). Near the funnel flow, level five experiences higher level of turbulence which modifies the wake dynamics (increase of 8–15% in turbulence intensity in BLI and 19–24% in BLII, in relation to the upper levels).

The multi-level spectral description of aerodynamic forces offers a convenient formulation for a random vibration-based, dynamic analysis of cylindrical structures. However, for computational convenience, mode-generalized spectral descriptions are customarily utilized. In this study, the mode-generalized alongwind and acrosswind spectra given in Figures 15 and 16 were obtained by summation of the measured signal observed at the five

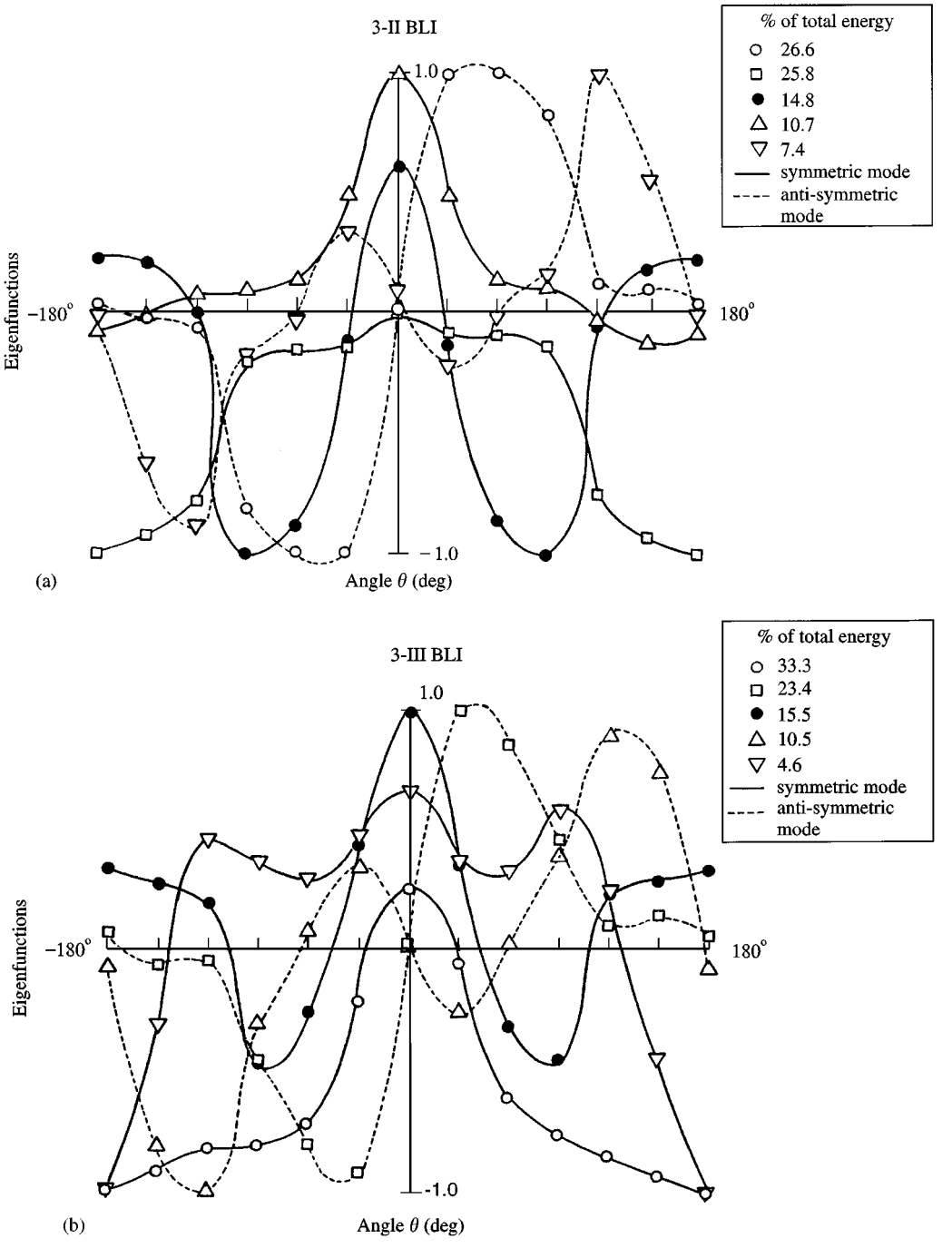

Figure 11. Eigenvector representation of pressure field in BLI: (a) 3-II and (b) 3-III.

levels of measurement. These spectra represent the fundamental mode-shape-weighted aerodynamic loads. The mode-generalized spectra reflects the characteristics of the multi-level spectra described in Figures 13 and 14. As noted earlier, the pressure tap in the wake of the first set of trip wires exhibits very large contribution in the low-frequency range, which is

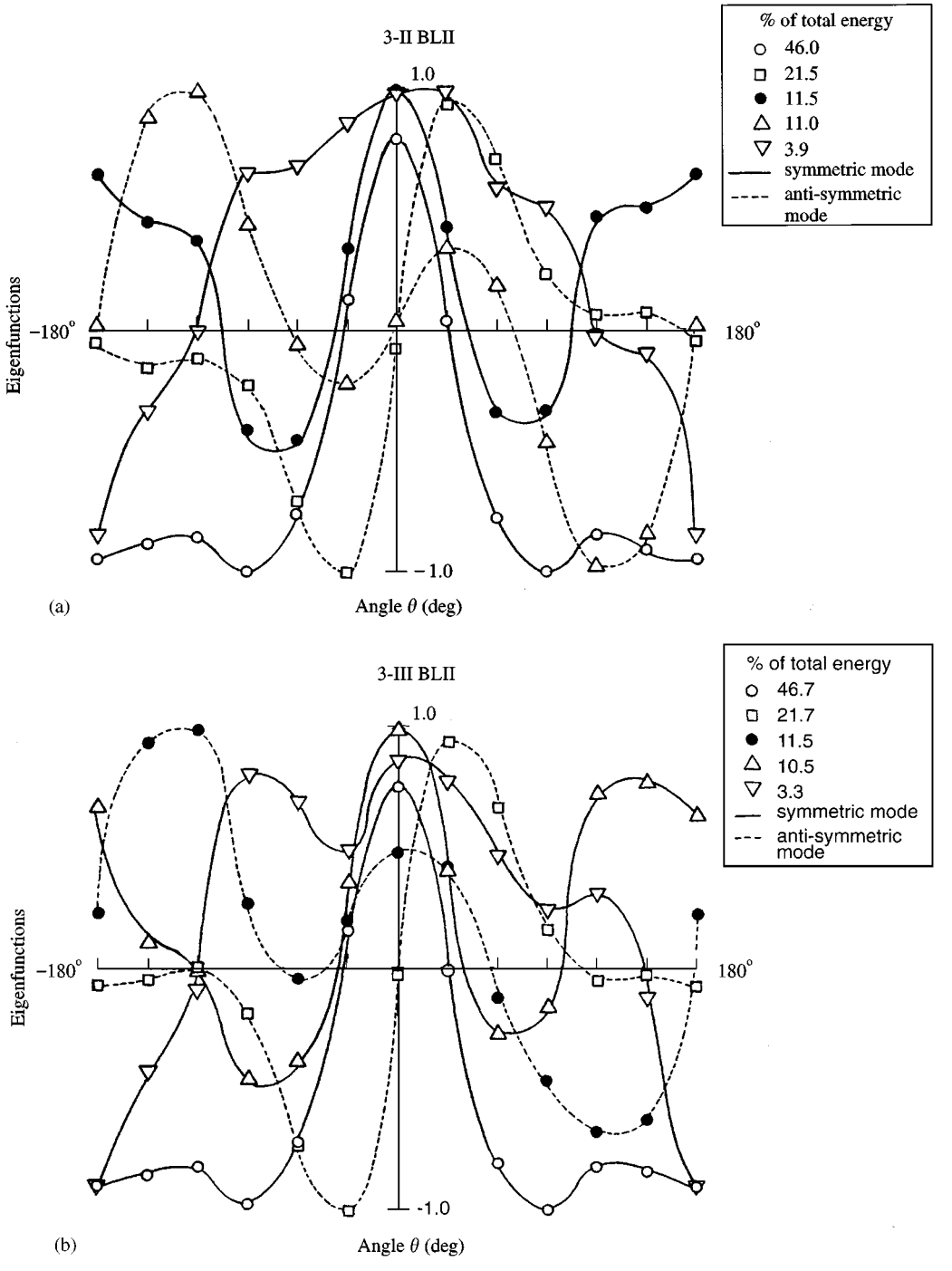

Figure 12. Eigenvector representation of pressure field in BLII (a) 3-II and (b) 3-III.

evident in the mode-generalized spectra. This is in the range of wind speeds at which self-excited loads become significant. Beyond this range, the wind speeds exceed any practical significance. In Figure 16, corrected spectral curves are presented. The corrected spectral description was obtained by a base pivoted rigid model mounted on instrumental

TABLE 4

Energy distribution of pressure fluctuation using eigenfunction analysis

Model	Boundary layer	Percent total energy in ith mode					Percent of total energy counted
		1	2	3	4	5	
3-I	I	44·3	24·2	12·9	9·5	4·1	95·0
3-II	I	26·6	25·8	14·8	10·7	7·4	85·3
3-III	I	33·3	23·4	15·5	10·5	4·6	87·3
3-I	II	47·4	22·5	12·5	9·3	3·3	95·0
3-II	II	46·0	21·5	11·5	11·0	3·9	93·9
3-III	II	46·7	21·7	11·5	10·5	3·3	93·7

leaf springs. The model surface was equipped with roughness wires. Measuring the forces directly from an oscillating model eliminated most of the low-frequency contributions to the force spectra introduced by the presence of wires and picked up by the adjacent pressure taps. This resulted in a bias in the spectra at low frequencies due to the weighting of a tap near the wires to the overall load spectra at that level. Details of the measurements and correction are given in Kareem & Cheng (1984). In both the alongwind and acrosswind spectra, the influence of added incident turbulence broadened the spectral description. In the acrosswind spectra, lowering of the spectral peak was also noted. The corrected spectra were also compared with full-scale measurements by Ruscheweyh & Hirsch (1975) in Figure 17. It is obvious that the roughened cylinder provides a good match of the full-scale spectrum.

The Strouhal number associated with each level of the measured acrosswind force spectrum indicated that it was not uniformly distributed as expected in a two-dimensional uniform flow (Figure 18). Level four represented the largest value, and it decreased for levels located near the free end as well as the base of the model. This could be attributed to the changes in the wake that took place at these respective locations as a result of proximity to the downwash at the free-end and the horse-shoe vortex near the tunnel flow. A similar trend was reported by Okamoto & Yagita [see Sakamoto & Arie (1983)], Rooney & Peltzer (1982) and others [e.g. Maull & Young (1972), Shaw & Star (1972), Stansby (1976)] in their measurements on finite length cylinders or two-dimensional cylinders in shear flows.

The local r.m.s. acrosswind force coefficients are given in Figure 19. The mode-generalized acrosswind force coefficients were found to be 0·0552 (0·0218) and 0·0565 (0·0328) for BLI and BLII, respectively, whereas the local acrosswind force coefficients varied between 0·14–0·16 for BLI and 0·14–0·21 in BLII [acrosswind force coefficient $= F_{\text{acrosswind}}/(\frac{1}{2}\rho U_H^2 A)$, in which ρ is the air density, U_H the mean wind speed at cylinder height, and A the projected area in the acrosswind direction]. The numbers in parenthesis represent the corrected values similar to the corrections in Figure 16. These values are in agreement with full-scale data (Hansen 1981; Sageau 1978), especially for the case of BLI which is similar to the site conditions. These values are slightly larger than those observed for the smooth cylinder (Kareem *et al.* 1989). In general, these values are lower than those observed in two-dimensional flow studies using smooth cylinders.

The spanwise broad- and narrow-band correlations of the aerodynamic forces at different levels were computed. In Figure 20 broad-band alongwind spanwise correlation is plotted along with results from the smooth cylinder analysis. In BLI, the smooth cylinder exhibits higher correlation, while the trend reverses in BLII. Overall, considering the average of both

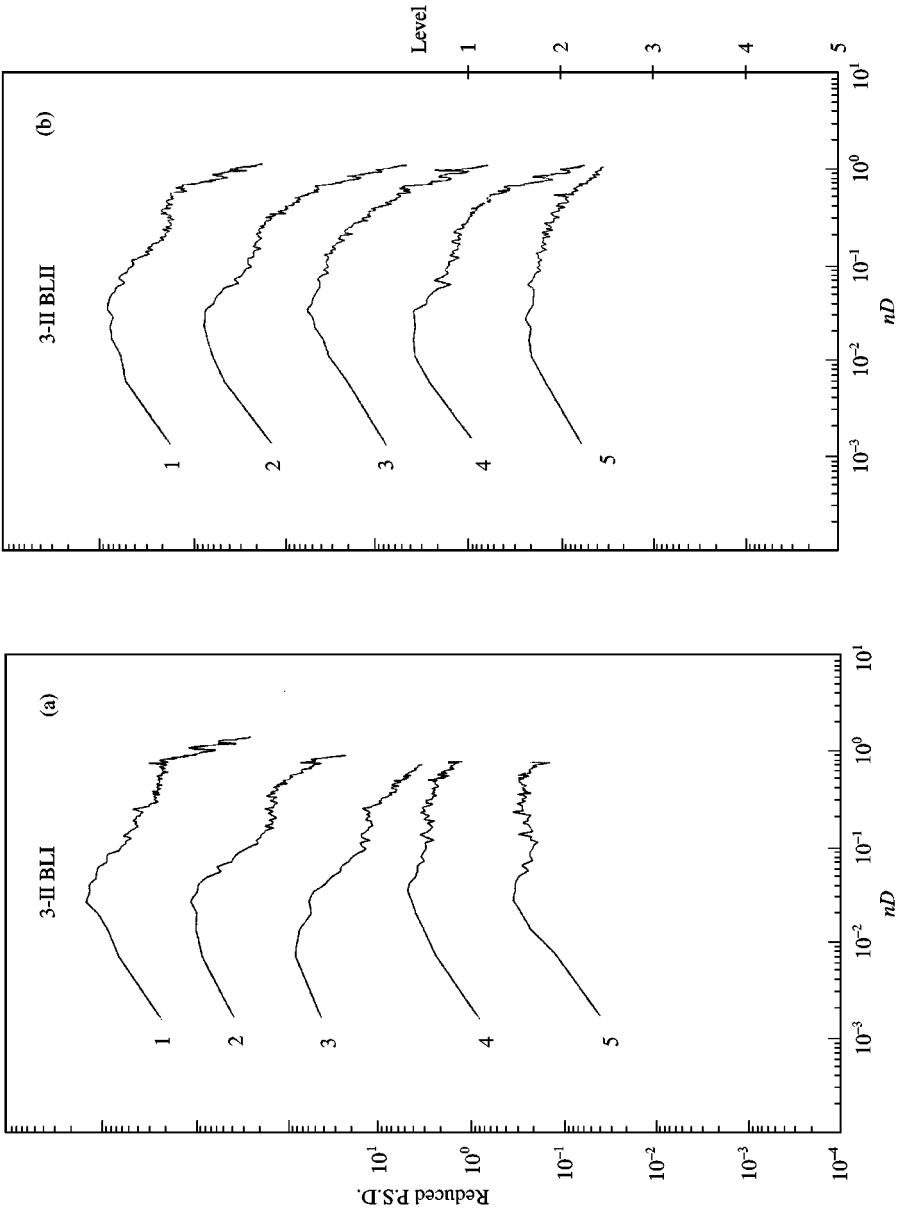

Figure 13. Alongwind force spectra at various levels (3-II) in BLI and BLII.

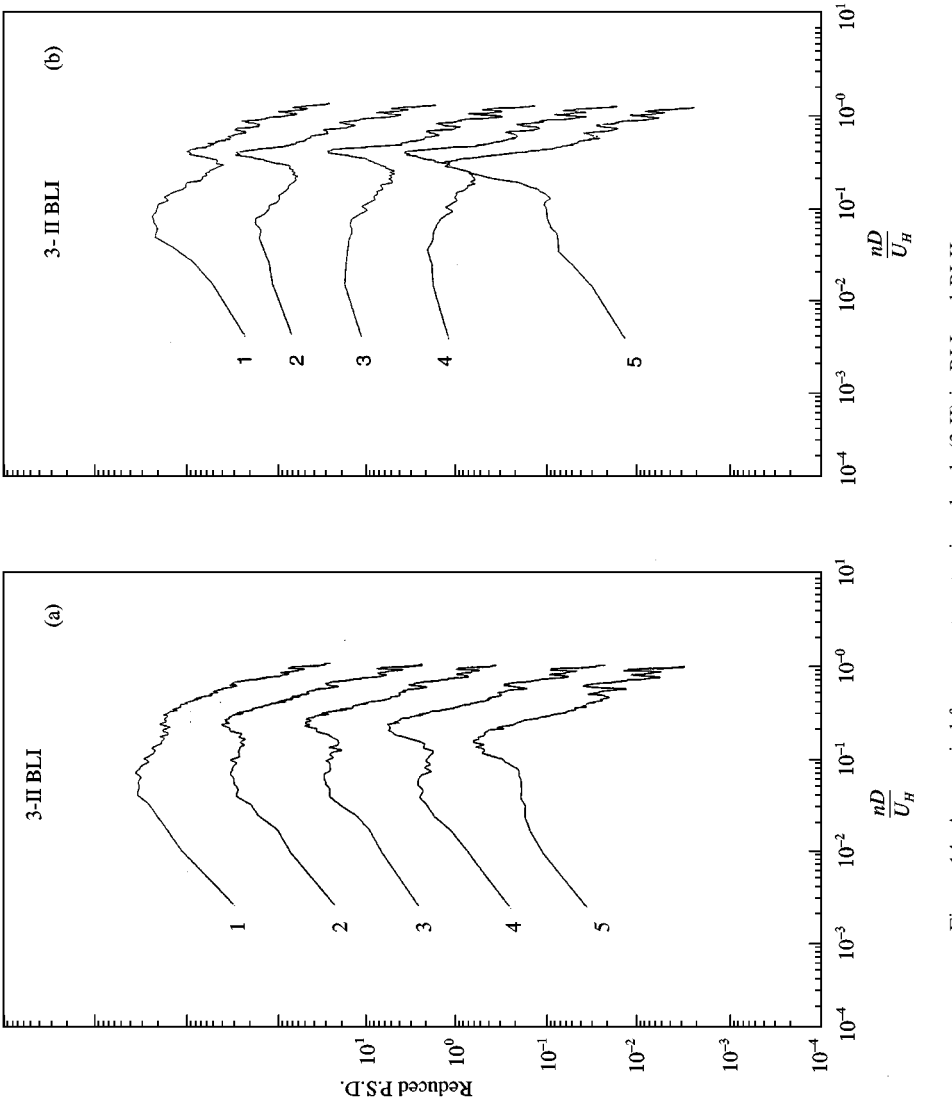

Figure 14. Acrosswind force spectra at arious levels (3-II) in BLI and BLII.

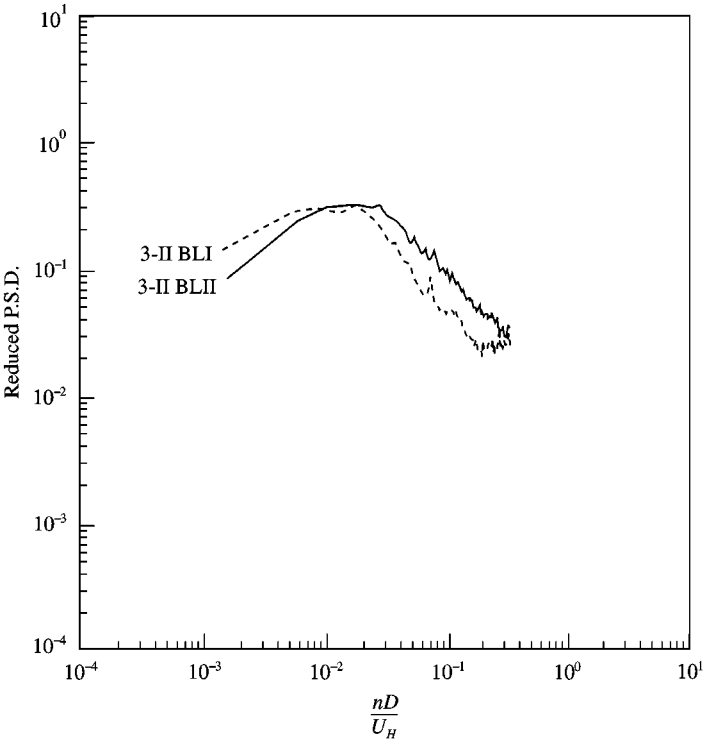

Figure 15. Mode-generalized alongwind spectra in BLI and BLII (3-II).

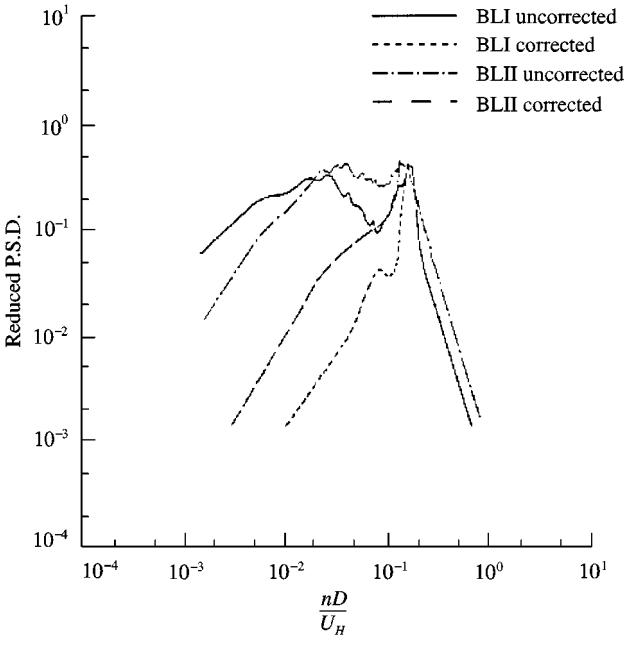

Figure 16. Mode-generalized acrosswind spectra in BLI and BLII (3-II).

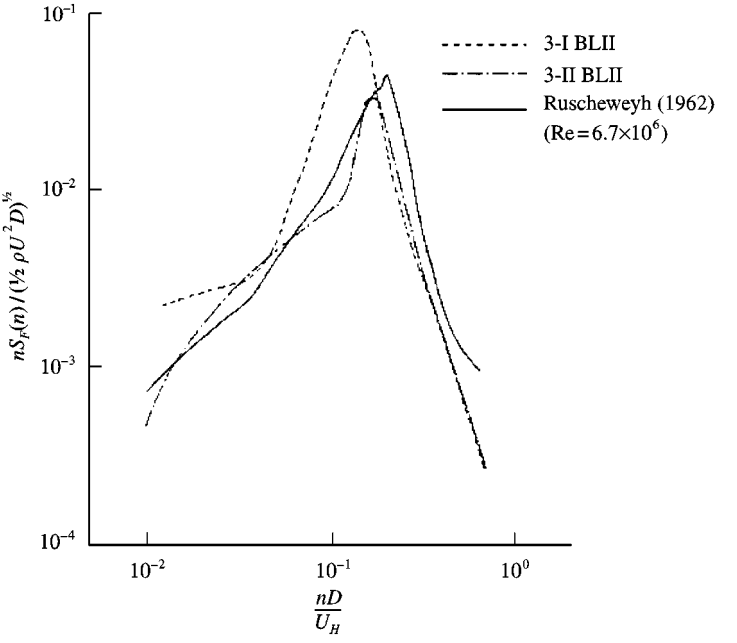

Figure 17. Comparison of acrosswind force spectra with a full-scale measurement.

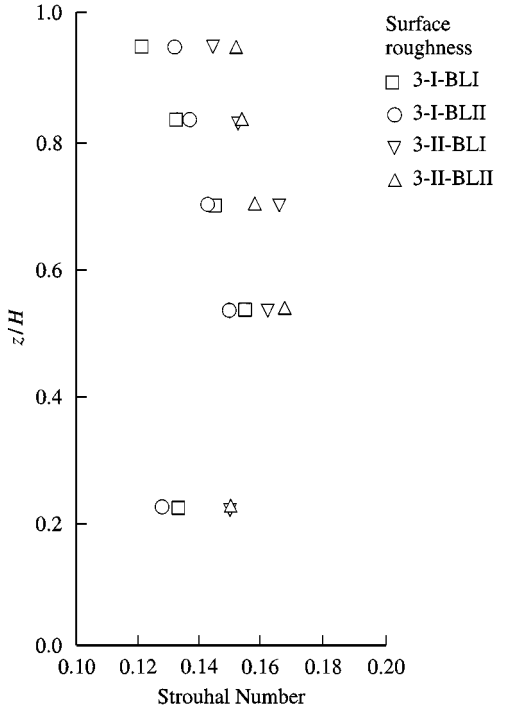

Figure 18. Variation of Strouhal number with height.

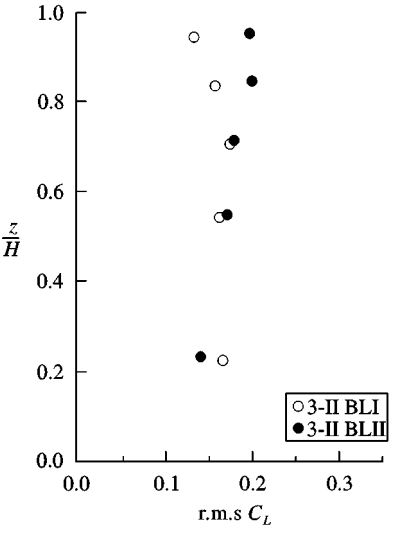

Figure 19. Variation of local r.m.s. acrosswind for coefficient.

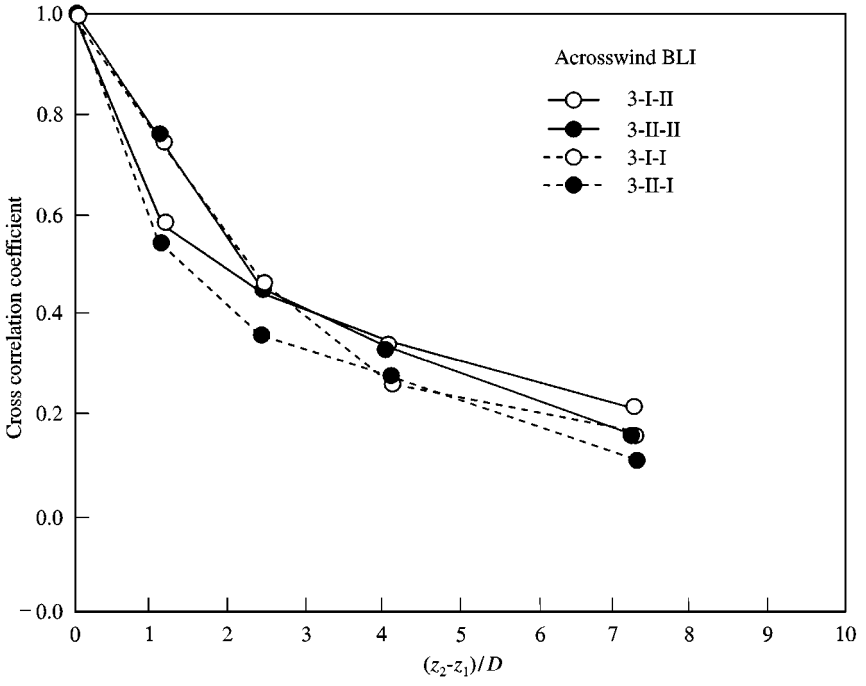

Figure 20. Broad-band alongwind spanwise force correlation in BLI and BLII.

cases, higher correlation is noted in BLII flow. In the acrosswind direction, higher values of broad-band correlation are noted for the roughened cylinder in BLI (Figure 21). A similar trend was noted for the acrosswind narrow-band correlation evaluated at the Strouhal frequency (Figure 22).

The spanwise broad-band correlation lengths are $2{\cdot}69D$ and $2{\cdot}19D$ for BLI and BLII flow, respectively. These values are higher than those observed for the smooth cylinder case ($2{\cdot}05D$ and $1{\cdot}77D$ for BLI and BLII, respectively). The narrow-band values are smaller than the broad-band case, $2{\cdot}03D$ and $1{\cdot}98D$ for BLI and BLII, respectively. Unlike the pressure correlation length scales, the presence of higher level of turbulence in BLII tends to reduce both broad- and narrow-band correlation. This is a consequence of area averaging of the random pressure field.

4. CONCLUSIONS

This study has provided a possible direction for artificially simulating a high Reynolds number flow field around a cylinder at low Reynolds numbers that are generally achievable in low-speed boundary-layer wind tunnels. In the following, a summary of the findings is presented.

(i) Among the various surface roughness types considered for simulating the high Reynolds number flow around cylindrical structures in this study, the two-dimensional roughness elements of $d/D = 0{\cdot}0067, 0{\cdot}02$ at $\theta = \pm 65,\ \pm 115^\circ$ best simulated the transcritical flow around the surface of a circular cylinder at a Reynolds number as low as $2{\cdot}5 \times 10^4$. The surface pressure measured on the model with the optimal surface roughness elements has the characteristics of high Reynolds number flow. The wake exhibits three-dimensional

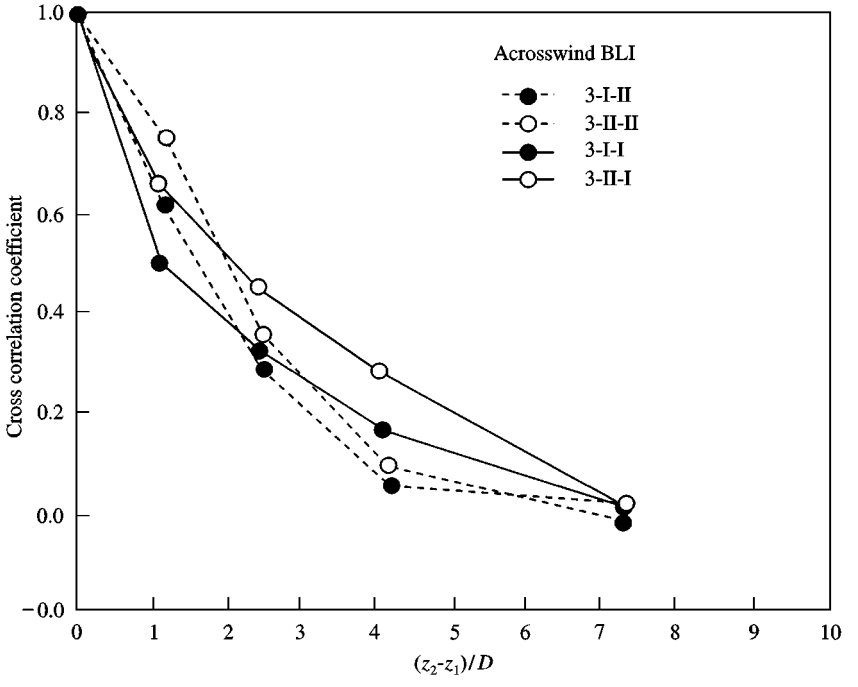

Figure 21. Broad-band acrosswind spanwise force correlation in BLI and BLII.

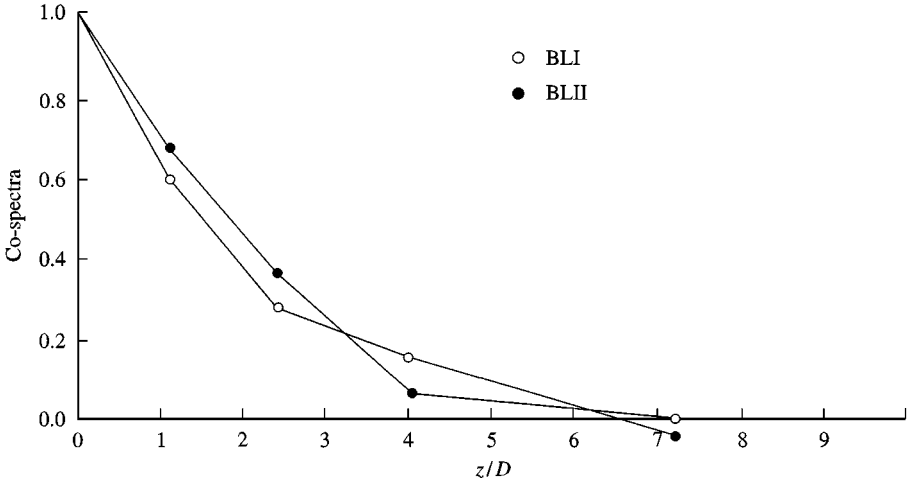

Figure 22. Narrow-band acrosswind spanwise force correlation in BLI and BLII.

features and has a spanwise pressure correlation length similar to those reported in full-scale measurements.

(ii) The r.m.s. pressure coefficients at the stagnation point are in good agreement with the strip and quasi-steady theories. The wake of forward wire introduces low-frequency oscillations in the proximity of the wire similar to those observed in flow over forward and backward step configurations. The addition of turbulence does not significantly influence

the spectral peaks at the Strouhal frequency. A follow-up study in a large high-speed wind tunnel showed for that a relatively larger test-section wind tunnel, the wire size can be reduced. This alleviated the concentration of low-frequency pressure oscillations in the wake of a wire (Cheng 1990).

(iii) The pressure fluctuations do not represent a distinct antisymmetric circumferential correlation. The experiments generally reported in the literature involving two-dimensional cylinders exposed to low tubulence intensity and/or small-scale turbulence are dominated by antisymmetric correlation. This suggests that, for circular cylinders in atmospheric boundary layers, the vortex shedding process does not particularly dominate the surface fluctuating pressure field. The lateral velocity fluctuations associated with a high level of turbulence intensity in the approach flow also contributes to the pressure fluctuations.

(iv) The spanwise broad-band correlation length of the pressure fluctuations reflects the characteristics of the approach flow, i.e., higher correlation in BLII as compared with BLI. The narrow-band correlation centered at the Strouhal frequency, which represents the spatial correlation of vortex shedding, is vitiated in the presence of a higher level of turbulence in the approach flow.

(v) The eigenfunction analysis of the covariance expansion of pressure fluctuations on the model surface shows that the first five modes contribute 85–95% of the total energy. Among them, the vortex shedding, characterized by antisymmetric mode shapes, contributes 33–35% of the total energy. The eigenfunction analysis agrees with the observation that the circumferential pressure fluctuations do not predominantly exhibit antisymmetric correlation, and thus are not dominated by vortex shedding.

(vi) The manifold-pneumatic averaging of the fluctuating pressure field, in conjunction with the appropriate selection of the circumferential pressure tap locations, and the spanwise spacing, provides a direct measure of the corresponding mode-generalized aerodynamic force spectrum acting on the cylinder.

(vii) Local and mode-generalized spectra and aerodynamic force coefficients measured on a cylinder with surface roughness match most full-scale measurements. One of the drawbacks of the discrete roughness elements is that low-frequency fluctuations are introduced, thus affecting generalized force coefficients and spectra. These were corrected in this study. The best way to eliminate this local effect of the roughness elements would be to conduct experiments at higher Reynolds numbers. This would permit the use of a smaller roughness element size, thus minimizing or eliminating local effects. This alternative has been shown to work successfully (Cheng 1990).

(viii) Both broad- and narrow-band correlation lengths of the acrosswind force at different levels along the model height are reduced in the presence of a higher level of turbulence in the approach flow. A similar trend was observed for a smooth cylinder.

ACKNOWLEDGEMENTS

The support for this work was provided in part by the NSF Grants BCS 90-96274 and CMS95-03779 and ONR Grant No. N00014-93-0761. The authors are grateful to Professor P. C. Lu of Tamkang University for his assistance during this study.

References

Achenbach, E. & Heinecke, E. 1981 On vortex shedding from smooth and rough cylinders in the range of Reynolds number 6×10^3 and 5×10^6. *Journal of Fluid Mechanics* **109,** 239–252.

Armitt, J. 1968 Eigenvector analysis of pressure fluctuations on the West Burton instrumented cooling tower. Central Electricity Research Laboratories Note RP/L/N, 114.

Ayoub, A. & Karamcheti, K. 1982 An experiment on the flow past a finite cicular cylinder at high subcritical and supercritical Reynolds numbers. *Journal of Fluid Mechanics* **118,** 1–26.

Batham, J. P. 1973 Pressure distribution on circular cylinder at critical Reynolds numbers. *Journal of Fluid Mechanics* **57,** 209–228.

Bruun, H. H. & Davies, P. O. A. L. 1975 An experimental investigation of the unsteady pressure forces on circular cylinder in a turbulent cross flow. *Journal of Sound and Vibration* **40,** 535–559.

Cermak, J. E. 1971 Laboratory simulation of the atmospheric boundary layer. *AIAA Journal* **9,** 1746–1754.

Cheng, C.-M. 1990 Aerodynamic modeling and chimneys. In *Proceedings of Structures Congress 1990*, San Francisco. New York: ASCE.

Christensen, D. 1977 Wind forces on excitation of a 130 m concrete chimney. Series Paper 15, Institute of Hydrology and Hydraulic Engineering, University of Denmark.

Davenport, W. B. & Root, W. L. 1958 *An Introduction to the Theory of Random Signals and Noise*. New York: McGraw-Hill.

Farabee, T. M. & Casarella, M. J. 1986 Measurements of fluctuating wall pressure for separated/reattached boundary layer flows. In *Shear Flow-Structure Interaction Phenomena* (eds A. Akay & M. M. Reischman), pp. 17–25, New York: ASME.

Farell, C. 1981 Flow around fixed circular cylinder: fluctuating load. *ASCE Journal of Engineering Mechanics Division* **107,** 565–588.

Guven, O., Farell, C. & Patel, V. C. 1980 Surface roughness effects on the mean flow past circular cylinders. *Journal of Fluid Mechanics* **68,** 673–701.

Howell, J. F. & Novak, M. 1979 Vortex shedding from circular cylinders in turbulent flow. In *Proceedings of the 5th International Conference on Wind Engineering* (ed. J. E. Cermak), Fort Collins, CO, U.S.A.

Kareem, A. 1978 Wind excited motion of buildings. Ph.D. Dissertation, Department of Civil Engineering, Colorado State University.

Kareem, A. & Cheng, C.-M. 1984 Acrosswind response of towers and stacks of circular cross-section. Report No. UHCE 84-5, Department of Civil Engineering, University of Houston.

Kareem, A., Cheng, C.-M. & Lu, P. C. 1989 Pressure and force fluctuations on isolated circular cylinders of finite height in boundary layer flows. *Journal of Fluids and Structures* **3,** 481–508.

Kareem, A. & Cermak, J. E. 1984 Pressure fluctuations on a square building model in boundary layer flows. *Journal of Wind Engineering and Industrial Aerodynamics* **16,** 17–41.

Lawson, T. V. 1982 The use of roughness to produce high Reynolds number flows around circular cylinder at low Reynolds numbers. Short Communication, *Journal of Wind Engineering and Industrial Aerodynamics* **10,** 381–387.

Loeve, M. 1977 *Probability Theory*, 4th Edition. New York: Springer-Verlag.

Lumley, J. L. 1965 The structure of inhomogeneous flows. In *Proceedings of the International Colloquium on Fine Scale Structure of the Atmosphere and its Influence on Radio Wave Propagation*, U.S.S.R. Academy of Science.

Maull, D. J. & Young, R. A. 1972 Vortex shedding from a bluff body in a shear flow. In *Flow Induced Structural Vibrations, IUTAM-IAHR Symposium* (ed. E. Naudascher), Karlsruhe, pp. 717–729. Berlin: Springer-Verlag.

Muller, F. P. & Nieser, H. 1976 Measurements of wind induced vibrations on concrete chimneys. *Journal of Wind Engineering and Industrial Aerodynamics* **1,** 239–247.

Nakamura, Y. & Tomorai, Y. 1982 The effects of surface roughness on the flow past a circular cylinder at high Reynolds number. *Journal of Fluid Mechanics* **123,** 363–378.

Naumann, A. & Quadflieg 1972 Vortex generation on a cylindrical building and its simulation in wind tunnel. In *Proceedings Flow Induced Structural Vibrations IUTAM/IAHR Symposium* (ed. E. Naudascher), Karlsruhe, pp. 730–747. Berlin: Springer-Verlag.

Rooney, D. M. & Peltzer, R. D. 1982 The effects of roughness and shear on vortex shedding cell length behind a circular cylinder. *ASME Journal of Fluids Engineering* **104,** 72–80.

Ruscheweyh, H. & Hirsch, G. 1975 Full-scale measurements of dynamic response of tower shaped structures. In *4th International Conference on Wind Effects on Buildings and Structures*, pp. 133–142, London, U.K.

Sadeh, W. Z. & Saharon, D. B. 1982 Turbulence effect on crossflow around a circular cylinder at subcritical Reynolds numbers. NASA Report 3622.

Sageau, J. F. 1978 In-situ study of the steady and fluctuating pressure fields around a 240 m high chimney. *Journal of Industrial Aerodynamics* **2,** 361–383.

SAKAMOTO, H. & ARIE, M. 1983 Vortex shedding from a rectangular prism and a circular cylinder placed vertically in a turbulent boundary layer. *Journal of Fluid Mechanics* **126,** 147–165.

SCHEWE, G. 1983 On the force fluctuations acting on a cylinder in cross flow from subcritical up to transcritical Reynolds numbers. *Journal of Fluid Mechanics* **133,** 265–285.

SCHLICHTING, H. 1960 *Boundary Layer Theory*. New York: McGraw-Hill.

SCHNABEL, W. 1981 Field and wind tunnel measurement of wind pressure acting on a tower. *Journal of Wind Engineering & Industrial Aerodynamics* **8,** 73–91.

SHAW, T. L. & STAR, M. R. 1972 Shear flows past circular cylinder. *ASCE Journal of Hydraulic Division* **98,** 461–473.

SHIH, W. C. L., WANG, C., COLES, D. & ROSHKO, A. 1993 Experiments on flow past rough circular cylinders at large Reynolds numbers. *Journal of Wind Engineering and Industrial Aerodynamics* **49,** 351–368.

STANSBY, P. K. 1976 The lock-on of vortex shedding due to the cross-stream vibration of circular cylinders in uniform and shear flows. *Journal of Fluid Mechanics* **74,** 641–665.

SURRY, D. 1972 Some effects of intense turbulence on the aerodynamics of circular cylinder at subcritical Reynolds numbers. *Journal of Fluid Mechanics* **52,** 543–563.

SZECHENYI, E. 1975 Subcritical Reynolds number simulation for two-dimensional flow over a circular cylinder. *Journal of Fluid Mechanics* **70,** 523–542.

TUNSTALL, M. J. 1970 Fluctuating pressure on circular cylinders in uniform & turbulent flows. Central Electricity Research Laboratories, Lab. Note No. RD/L/N, 45/70.

VAN NUNEN, J. W. G. 1972 Pressure and forces on a circular cylinder in a cross flow at high Reynolds numbers. In *Proceedings Flow Induced Vibrations*, *IUTAM-IAHR Symposium* (ed. E. Naudascher), Karlsruhe, pp. 749–754. Berlin: Springer-Verlag.

VICKERY, B. J. & CLARK, A. W. 1972 Life or acrosswind response of tapered stack. *ASCE Structural Division Journal* **98,** 1–20.